Journal of the Brazilian Society of Mechanical Sciences and Engineering (2021) 43:313
https://doi.org/10.1007/s40430-021-03018-0

TECHNICAL PAPER

Modelling and simulation of water vapor adsorption in silica gel bidisperse beds

Jailson Charles dos Santos[1] · João Alves de Lima[2] · José Maurício Gurgel[2] · Francisco Marcondes[3]

Received: 17 June 2020 / Accepted: 4 May 2021 / Published online: 26 May 2021

Abstract

Desiccant cooling systems are widely recognized as an alternative technology to vapor compression cooling. Desiccant systems are attractive for air conditioning applications due to the possible use of low-grade heat and green refrigerants in their operation. In such systems, air dehumidification is achieved using bed compacted with desiccant materials such as silica gel, activated alumina, and zeolite. Desiccant systems, on the other hand, present a low coefficient of performance due to the poor heat and mass transfer in the adsorbent bed. A way to enhance the heat and mass transfer in desiccant systems can be accomplished by optimizing the adsorbent packing in the bed. This paper presents a numerical investigation of the dynamics of water vapor adsorption in silica gel bidisperse bed. The adsorbent bed is compacted with particles of two different sizes to reduce the voids between the adsorbent particles and hence increase the amount of desiccant and the adsorbed water mass in the bed. The effect of bidisperse packing in the air dehumidification capacity and adsorbed water mass is studied. The influence of the pressure drop applied on the adsorbent column and the inlet air conditions in the dehumidification process is also investigated. The numerical results showed that bidisperse packing increases the dehumidification capacity (improvement of 22.9%) and the amount of water adsorbed (improvement of 25%) in the bed compared to the case where monodisperse packing is applied to the system, contributing to the improvement in the performance of desiccant beds in air conditioning applications.

Keywords Air conditioning · Desiccant bed · Bidisperse packing · Numerical model · Simulation

List of symbols

C_p	Specific heat at constant pressure (J/kg K)
C_S	Volumetric heat capacity of the adsorbent (J/m^3 K)
d	Diameter of the small pellet (m)
d_{av}	Average diameter of the pellets (m)
D	Diameter of the large pellet (m)
D_{S0}	Pre-exponent constant (m^2/s)
D_L	Axial dispersion coefficient (m^2/s)
E_a	Activation energy (J/kg)
q	Concentration of water vapor in adsorbent (kg/kg)
$\overline{q}$	Instantaneous water concentration in the adsorbent particle (kg/kg)
u	Interstitial velocity (m/s)
h_p	Fluid-particle heat transfer coefficient (W/m^2 K)
ΔH	Heat of adsorption (J/kg)
L	Column length (m)
m	Mass flow rate (kg/s)
Nu	Nusselt number
p	Moist air pressure (Pa)
K	Bed permeability (m^2)
Pr	Prandtl number
R	Radius (m)
Re	Reynolds number
R_g	Ideal gas constant (J/kg K)
t	Time (s)
T	Temperature (K)
U_g	Overall heat transfer coefficient (W/m^2 K)
W	Humidity ratio (kg/kg)
x	Axial coordinate in column (m)
x_D	Volumetric fraction of the large pellet

Technical Editor: Monica Carvalho.

✉ Jailson Charles dos Santos
jailson.charles@urca.br

[1] Department of Mechanical Production Engineering, Regional University of Cariri, Av. Leão Sampaio, 107, Juazeiro do Norte, Ceará 63040-000, Brazil

[2] Center of Alternative and Renewable Energy, Solar Energy Laboratory, Federal University of Paraiba, Cidade Universitária, João Pessoa, Paraíba 58051-900, Brazil

[3] Department of Metallurgical Engineering and Material Science, Federal University of Ceará, Campus do Pici, Bloco 714, Fortaleza, Ceará 60455-760, Brazil

Greek letters

ε	Bed porosity (interparticle)
ε_D	Fractional porosity of the large pellet
ε_d	Fractional porosity of the small pellet
ε_{pD}	Porosity of the large pellet (intraparticle)
ε_{pd}	Porosity of the small pellet (intraparticle)
λ	Thermal conductivity (W/m K)
ρ	Density (kg/m^3)
τ	Bed tortuosity
μ	Moist air viscosity (kg/m s)
δ	Particle size ratio ($\delta = d/D$)
η	Dehumidification efficiency

Subscripts

∞	Relative to the ambient
0	Relative to the initial condition
d	Small pellet
D	Large pellet
e	Relative to the external surface
f	Relative to the fluid phase
in	Relative to the column inlet
p	Relative to the pellet
S	Relative to the solid phase
v	Water vapor
w	Relative to the adsorbed water

Superscripts

*	Relative to the adsorption equilibrium

1 Introduction

Sustainable development has been a common goal by all the nations around the world. Nevertheless, economic and population growth imposes an increase in energy consumption and therefore reduces the natural resources available in our planet. Conventional sources of energy are those based on carbon (oil, gas, and coal) and represent about 80% of world energy production, according to data from the International Energy Agency (IEA). The exploitation of these energy resources is also associated with the emission of an increasing amount of gases that cause global warming, especially carbon dioxide. Another issue is that these energy sources are not renewable and the possibility of depletion of these resources poses a clear threat to the sustainability of human civilization [1, 2].

Economic growth, which improve the living standards of peoples, has generated a growing demand for air conditioning equipment. This has had a considerable impact on energy consumption. About 45% of the primary energy consumed in residential and commercial buildings is estimated to be attributed to the operation of these machines [3]. The vast majority of air conditioning systems traditionally used in thermal comfort applications operate on a vapor compression refrigeration cycle.

Vapor compression refrigeration systems have two main disadvantages that make them impossible to remain in use in the current scenario: First, these systems require the supply of electricity for their operation, often obtained by burning fossil fuels. The second issue is that vapor compression refrigeration systems use chlorofluorocarbons (CFCs), hydrochlorofluorocarbons (HCFCs), and hydrofluorocarbons (HFCs) as refrigerants in their work cycles. Chlorofluorocarbons and hydrochlorofluorocarbons have a direct effect on the destruction of the ozone layer while hydrofluorocarbons have a high potential for global warming often greater than that of carbon dioxide [2].

A promising alternative solution for replacing vapor compression refrigeration machines is the desiccant cooling system. These systems have the advantage of using water as a refrigerant in their work cycle, as well as the possibility of using low-grade energy such as waste heat and solar energy. The operation of these systems is based on desiccant dehumidification and evaporative cooling processes. In these systems, air is dehumidified when in contact with adsorbent materials such as silica gel, zeolite, and activated alumina. These materials act on the retention of water vapor molecules (adsorption) present in the air on the inner surface of their pores [4, 5]. One advantage of the desiccant system is that the latent load is removed separately of the sensible load. Desiccant material removes the latent load, while the sensible load is removed in the evaporative cooling unit or in other processes such as heat recovery/regeneration. This procedure allows the use of different energy sources to separately remove these thermal loads. Therefore, the advantage is the possibility of using low-grade energy to remove the latent load in order to reduce the use of conventional energy in the dehumidification process [6].

The process of air dehumidification must be continuous; therefore, when the desiccant matrix is saturated with moisture, it must be regenerated through contact with hot air. In order to have a continuous process there should exist two streams: one to regenerate the desiccant matrix (regeneration air) and another one for air dehumidification (process air). In general, two methods are largely used. One uses two or more fixed adsorbent beds that operate in alternating cycles of adsorption and desorption through the use of a simple control valve [7]. The second process consists of the use of a desiccant rotor that continuously rotates between process and regeneration air streams. In this case, while the rotor regeneration section is exposed to the hot air, expelling moisture absorbed from the air in the previous process, the rotor adsorption section dehumidifies the process air, removing its moisture [8]. Although desiccant rotors are effective in the air dehumidifying process, according to Yeboah

and Darkwa [9], packed beds are usually free of mechanical problems due to their non-moving parts and provide a high volume of adsorbent for fluid–solid interaction. Additionally, the bidisperse packing proposed here to the adsorbent bed would be easier to implement using a packed bed. For the above reasons, a desiccant packed bed will be applied in our study.

Despite their advantages, desiccant cooling systems have a low coefficient of performance (COP < 1) due to the low rate of heat and mass transfer in the adsorbent bed and therefore are not currently competitive with vapor compression refrigeration machines. Adsorption is an exothermic phenomenon that causes an increase in the temperature of the adsorbent, which in turn results in a reduction of the amount of adsorbed water in the dehumidification process. Also, due to the low conductivity of the adsorbent bed (~ 0.1–0.4 W/m K), the heat transfer in the bed is poor and therefore reduces the performance of the cycle [10]. Another key issue of desiccant cooling is the poor mass transfer in the adsorbent due to the low mass diffusivity of adsorbent-adsorbate pairs (~ 10^{-8} to 10^{-14} m^2/s), which reduces the system dehumidification capacity [11]. These restrictions in heat and mass transfer processes result in large and heavy air conditioning systems. Intensification of the heat and mass transfer processes in the bed can be achieved by the use of efficient packing methods. In this regard, bidisperse packing can be used to reduce void spaces in the bed and to increase the mass of compacted adsorbent per unit of volume. Such an approach not only allows the increase of the adsorbed water mass, but also the increase of coefficient of performance (COP) of desiccant cooling system [12].

The packing structure of the adsorbent bed affects several important variables in the adsorption process such as: interparticle porosity, permeability, tortuosity, flow rate, pressure drop, breakthrough time, fluid-particle heat transfer coefficient, and packing density, among others. Many works addressing the permeability and porosity of bidisperse beds are available in the literature [13–20]. According to Dias et al. [19], the interparticle porosity of the bidisperse bed depends on the ratio between the diameter of the small (d) and large (D) particles, $\delta = d/D$, and on the volumetric fraction occupied by the large particles in the bed, x_D, and monosize component porosities. By reducing the particle size ratio, $\delta = d/D$, the interparticle porosity of the bed decreases and the packing density increases, when x_D is fixed. The permeability, in turn, depends on the interparticle porosity and tortuosity of the bed. Other authors have studied the effect of the packing structure on the effective thermal conductivity of the bed [21, 22]. However, few studies addressing the effect of the packing structure on the adsorption dynamics in packed beds have been carried out. Chang [23] carried out an experimental study to investigate the adsorption of natural gas in an activated carbon bidisperse bed. The results showed that the packing density of the bidispersed bed is higher than that obtained with the monodisperse packing of large or small particles (improvement of 25%). The results also showed that when a ratio between the sizes of the adsorbent particles (D/d) of 7/1 was used, the bed adsorption capacity was significantly improved in relation to the case of monodisperse packing using large particles alone. Shirley and LaCava [24] carried out an experimental study of the performance of the PSA (Pressure Swing Adsorption) separation process for extracting nitrogen from the air using an activated carbon bed with bidisperse packing. The experimental results showed that the diameter ratio between the large and small particles, the diameter of the small particles, and the percentage of volume of the small particles in the bed are all critical for the optimization of the PSA process. Santos et al. [25] developed a numerical study of the methane adsorption dynamics in activated carbon bidisperse bed. Five particle size ratios (d/D) were studied: 1 (monodisperse packing), 1/5, 1/10, 1/15, and 1/20. The effect of the gas inlet temperature and the pressure drop applied in the methane storage capacity was also investigated. The results showed that the use of bidisperse packing increased the packing density by 30% and the methane storage capacity by 20% when δ=1/20, compared to the case of monodisperse packing ($\delta = 1$) with small particles only. For the cases investigated, δ = 1/10 showed a good compromise between storage capacity (16% gain over the monodisperse bed) and required charging time (about 500 s), being identified as the optimal size ratio for application in methane storage vessels. The results also showed that the charging time in the bed can be optimized by the pressure drop applied and the storage capacity can be increased by reducing the temperature of the gas admitted to the bed. Girnik and Aristov [12] investigated, for the first time, the effect of a bidisperse adsorbent bed in the dynamics of water vapor in an adsorption chiller. The authors performed experiments in a bidisperse bed obtained by compacting large (0.8–0.9 mm) and small (0.20–0.25 mm) particles of the AQSOA-FAM-Z02 adsorbent. It was observed that the mixing of large and small pellets in the packing increased the adsorbed water mass by 21% compared to the system in which the packing was obtained with the large particles alone (monodisperse packing). There are several numerical and experimental investigations of water vapor adsorption in monodisperse silica gel beds [26–35]. However, to the best of our knowledge, there are no studies in the literature addressing the adsorption dynamics of water vapor in silica gel beds with bidisperse packing for air conditioning applications. Therefore, the main focus of this work is the development of a numerical model to investigate the effect of the application of bidisperse packing in the air dehumidification capacity using silica gel desiccant packed beds operating under different conditions of the process air (temperature, humidity, and flow rate). Herein, silica gel was

chosen because of its suitability for low-grade heat source (regeneration temperature below 100 °C) and good cycle stability. The effect of the particle size ratio on the pressure drop across the adsorbent bed will also be investigated. It is further intended to show that the use of different sizes of adsorbent particles can make the bed much more compact and offer substantial gains in the removal of moisture from the air. The direct benefit of this application would be the enhancement of the coefficient of performance (COP) in desiccant cooling systems and the development of more efficient and compact air conditioning machines.

2 Mathematical model

Figure 1 shows the bidisperse column of silica gel used for air dehumidification. The column is filled up with silica gel particles of two different sizes (D and d) to obtain a bidisperse packing with a regular and homogeneous structure. The moist air flows from one side of the column to the other. During the adsorption process, water vapor is adsorbed in the silica gel bed, and the air at the outlet of the column is dehumidified and heated because of the adsorption heat. Next, we show the equations that describe the dynamics of water vapor adsorption in the bidisperse column.

2.1 Porosities and packing density in bidisperse beds

The interparticle porosity of the bed, ε, the fractional porosity of small particles, ε_d, the fractional porosity of large particles, ε_D, and the intraparticle porosity of large and small particles, $\varepsilon_{\mathrm{pD}}$ and $\varepsilon_{\mathrm{pd}}$, in conjunction with packing density in bidisperse beds, ρ_b, are defined in Santos et al. [25].

2.2 Column model

For the column model, the following assumptions are considered:

- radial effects are negligible;
- moist air is considered as a mixture of dry air and water vapor which obeys Dalton's law;
- moist air and water vapor behave as ideal gases;
- local thermal non-equilibrium is assumed between the air and the adsorbent. Therefore, distinct energy balances are used for description of the heat transfer in the moist air flow and adsorbent particles.

The heat and mass transfer in silica gel bidisperse bed are described by the mass balances to the moist air and to the water vapor (Eqs. 1, 2), momentum (Eq. 3), energy balance to the moist air (Eq. 4), and the ideal gas equation to the moist air (Eq. 5).

$$\frac{\partial \rho_f}{\partial t} + \frac{\partial}{\partial x}\left(\rho_f u\right) = -\frac{\rho_S\left(1-\varepsilon_d\right)\varepsilon_D(1-\varepsilon_{pd})}{\varepsilon}\frac{\partial \overline{q}_d}{\partial t} - \frac{\rho_S\left(1-\varepsilon_D\right)(1-\varepsilon_{pD})}{\varepsilon}\frac{\partial \overline{q}_D}{\partial t} \tag{1}$$

$$\frac{\partial \rho_v}{\partial t} + \frac{\partial}{\partial x}\left(\rho_v u\right) = \frac{\partial}{\partial x}\left(D_L\frac{\partial \rho_v}{\partial x}\right) - \frac{\rho_S\left(1-\varepsilon_d\right)\varepsilon_D(1-\varepsilon_{\mathrm{pd}})}{\varepsilon}\frac{\partial \overline{q}_d}{\partial t} - \frac{\rho_S\left(1-\varepsilon_D\right)(1-\varepsilon_{\mathrm{pD}})}{\varepsilon}\frac{\partial \overline{q}_D}{\partial t} \tag{2}$$

$$\frac{\partial}{\partial t}\left(\rho_f u\right) + \frac{\partial}{\partial x}\left(\rho_f\, u\, u\right) = -\frac{\partial p}{\partial x} - \frac{\mu\,\varepsilon\, u}{K} - \frac{C_F\rho_f\,\varepsilon^2\,u^2}{\sqrt{K}} \tag{3}$$

$$\frac{\partial}{\partial t}\left(\rho_f T_f\right) + \frac{\partial}{\partial x}\left(\rho_f\, u\, T_f\right) = \frac{\partial}{\partial x}\left(\frac{\lambda_f}{cp_f}\frac{\partial T_f}{\partial x}\right) + \frac{6\,h_{\mathrm{pd}}}{d}\frac{(1-\varepsilon_d)\,\varepsilon_D}{\varepsilon\, cp_f}(T_{\mathrm{sd}} - T_f) + \frac{6\,h_{\mathrm{pD}}}{D}\frac{(1-\varepsilon_D)}{\varepsilon\, cp_f}(T_{\mathrm{sD}} - T_f) + \frac{2U_g(T_\infty - T_f)}{\varepsilon\, R_i cp_f} \tag{4}$$

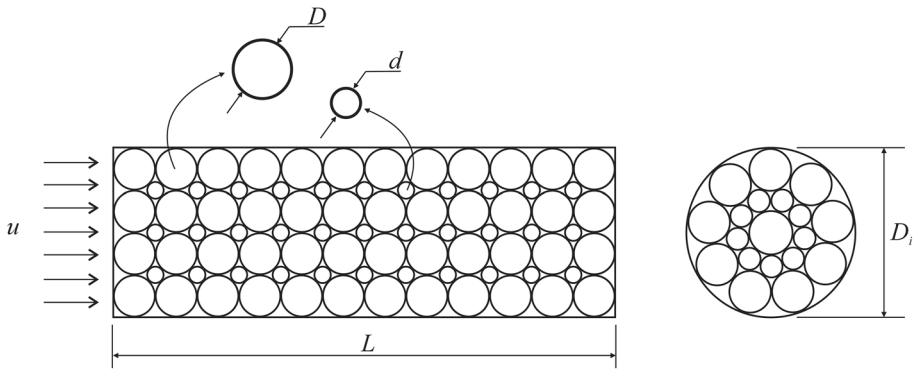

Fig. 1 Silica gel desiccant bed with bidisperse packing

$$\rho_f = \frac{p}{R_g\, T_f} \tag{5}$$

Equation (1) represents the mass balance to the moist air; the first term on the right-hand side represents the mass transfer from the moist air to the small adsorbent particles, while the second term represents the mass transfer to the large adsorbent particles. Equation (2) represents the mass balance to the water vapor flow. The first term on the right-hand side represents the axial dispersion of water vapor, while the second and third terms denote the transfer of water vapor to the small and large particles, respectively. The axial mass dispersion coefficient, D_L, is evaluated using the correlation suggested by Wakao and Funazkri [36]. In the momentum balance given by Eq. (3), K denotes the permeability of the porous media; we used the model given by Dias et al. [20]. The parameter C_F is chosen in order for the momentum equation to reproduce Ergun's equation when the steady state is reached. These two parameters are given by

$$K = \frac{\left(d_{\text{av}}\right)^2 \varepsilon^2}{\left(36\, K_0\, \tau^2 (1-\varepsilon)^2\right)} \tag{6}$$

$$C_F = \frac{1.75\, \varepsilon^{-3/2}}{\sqrt{150}} \tag{7}$$

In Eq. (6), d_{av} denotes the mean diameter of the particles used in the bidisperse packing given by Dias et al. [20]; K_0 is equal to 150/36 to satisfy Ergun's equation, and τ is the tortuosity of the porous media. Finally, in the energy balance, Eq. (5), the last three terms on the right-hand side represent the heat transfer from the moist air to the small particles, the heat transfer to the large particles, and the heat exchange between the column and the environment, respectively.

To study the adsorption process in the bidisperse bed, it is assumed that moist air with a prescribed pressure (p_{in}), temperature (T_{in}), and humidity ratio (W_{in}) is forced into the column, while the outlet pressure is kept constant at the initial value (p_0). The column is initially saturated with moist air at pressure p_0, temperature T_0, and humidity ratio W_0. The initial condition for the velocity field is $u_0 = 0$. Therefore, the initial and boundary conditions for the bed equations are given by

$$p(x,0) = p_0; T_f(x,0) = T_0; u(x,0) = u_0; W(x,0) = W_0 \tag{8}$$

$$p(0,t) = p_{\text{in}}; T_f(0,t) = T_{\text{in}}; W(0,t) = W_{\text{in}} \tag{9}$$

$$p(L,t) = p_0; \frac{\partial T_f(L,t)}{\partial x} = 0; \frac{\partial \rho_v(L,t)}{\partial x} = 0 \tag{10}$$

2.3 Pellet model

The following assumptions are used for the adsorbent pellets:

- pellets are spherical particles uniformly distributed;
- the mass transfer in the adsorbent particles is described by the linear driving force (LDF) model (Sakoda and Suzuki [37]);
- temperature is uniform inside the adsorbent particles. Our investigation will be performed to five particle size ratios (d/D = 1, 1/2, 1/5, 1/10, 1/13). For all simulations, we varied d and $D = 5$ mm was kept constant. The non-isothermal sorption in an adsorbent particle depends on the Lewis number (Le) and the thermal Biot number (Bi). According to Sun and Meunier [38], when Le > 10 the heat transfer inside the particle is very fast, and hence the temperature gradient into the particle may be neglected. For the cases investigated here, Le = 75.58, while the maximum value of Bi for the largest particle size ($D = 5$ mm) was equal to 0.06. Therefore, the uniform temperature assumption into the particle is justified. The thermophysical properties of the silica gel/water pair used to evaluate the Le and Bi numbers of the adsorbent particles were extracted from Gurgel et al. [39].
- adsorption equilibrium is attained in the external surface of the adsorbent particles.

The adsorbent bed is formed by the packing of large and small particles; therefore, the heat and mass transfer processes should be described separately for the two types of particles once the kinetics of sorption depends on the size of the pellets. For the large pellets, the mass and energy balances are given by

$$\frac{\partial \overline{q}_D}{\partial t} = \frac{15\, D_{S0}}{(D/2)^2} \exp\left(-\frac{E_a}{\overline{R}\, T_{SD}}\right)\left(q_D^* - \overline{q}_D\right) \tag{11}$$

$$C_{\text{SD}} \frac{\partial T_{\text{SD}}}{\partial t} = \frac{6\, h_{\text{pD}}}{D}\left(T_f - T_{\text{SD}}\right) + (-\Delta H)\rho_S\left(1 - \varepsilon_{\text{pD}}\right)\frac{\partial \overline{q}_D}{\partial t} \tag{12}$$

where q^* is the sorbate concentration evaluated at the equilibrium condition. In Eq. (11), E_a, D_{S0},$\overline{R}$, $q_D{}^*$ and $\overline{q}_{\text{D}}$, denote, respectively, the activation energy, the pre-exponential constant, the universal gas constant, the equilibrium concentration to water in the adsorbent, and the instantaneous water concentration in the adsorbent particle. The term $(15 D_{S0} \exp(-E_a/(\overline{R}\, T_{SD}))/((D/2)^2)$ in Eq. (11) is the overall mass transfer coefficient in the adsorbent particle as described by Sakoda and Suzuki [37]. In Eq. (12), C_{SD} is the effective total heat capacity that is given by the

mass-weighted average of the individual components in the particle (i.e., silica gel, adsorbed water, and water vapor).

$$C_{\mathrm{SD}} = \left[\rho_S\left(1-\varepsilon_{pD}\right)c_{ps} + \rho_S\left(1-\varepsilon_{\mathrm{pD}}\right)\overline{q}\,c_{pw} + \rho_v\,\varepsilon_{\mathrm{pD}}\,c_{pv}\right] \tag{13}$$

The following initial conditions for Eqs. (11) and (12) are, respectively, given by

$$\overline{q}_D(t=0) = q^*(p_0, T_0); T_{\mathrm{SD}}(t=0) = T_0 \tag{14}$$

For the small pellets, the mass and energy balances are similar to those given for the large pellets.

$$\frac{\partial \overline{q}_d}{\partial t} = \frac{15\,D_{S0}}{(d/2)^2}\exp\left(-\frac{E_a}{\overline{R}\,T_{\mathrm{Sd}}}\right)\left(q_d^* - \overline{q}_d\right) \tag{15}$$

$$C_{\mathrm{Sd}}\frac{\partial T_{\mathrm{Sd}}}{\partial t} = \frac{6\,h_{\mathrm{pd}}}{d}\left(T_f - T_{\mathrm{Sd}}\right) + (-\Delta H)\rho_S\left(1-\varepsilon_{\mathrm{pd}}\right)\frac{\partial \overline{q}_d}{\partial t} \tag{16}$$

The initial conditions for Eqs. (15) and (16) are given by

$$\overline{q}_d(t=0) = q^*(p_0, T_0); T_{\mathrm{Sd}}(t=0) = T_0 \tag{17}$$

2.4 Determination of heat transfer coefficients

The fluid-particle heat transfer coefficients, h_{pD} (large particle) and h_{pd} (small particle), as well as the overall heat transfer coefficient in the column wall, U_g, are determined according to the procedure described by Santos et al. [40].

2.5 Equilibrium isotherms

The properties of the adsorption equilibrium are described by the Tóth model (Tóth [41]) and it is given by Eq. (18).

$$q^*(p_v, T_S) = \frac{C_0\exp\left\{\Delta H/(R_v T_S)\right\}p_v}{\left[1+\left\{\frac{C_0}{q_\infty}\exp\left(\Delta H/(R_v T_S)p_v\right\}^n\right]^{1/n}} \tag{18}$$

In Eq. (18), C_0, q_∞, and n are constants, while ΔH, R_v, T_S, and p_v, denote, respectively, the adsorption heat, the ideal gas constant for the water vapor, the adsorbent temperature, and the water vapor partial pressure. The constants and parameters of Eq. (18) were extracted from Chua et al. [42].

3 Numerical method and code validation

The equations for the column model were discretized by the finite volume method [43, 44]. The pressure–velocity coupling is treated by the pressure implicit momentum explicit (PRIME) algorithm (Maliska [45]) in conjunction with a staggered arrangement to store the variables in the computational mesh. The properties at the interfaces of each control volume are evaluated through the weight upwind differencing scheme, Raithby and Torrance [46]. The linear systems were solved by the tridiagonal matrix algorithm. The velocities at the inlet and outlet of the column were calculated through the procedure suggested by Marcondes and Maliska [47]. The nonlinearities and couplings between the equations were solved through an iterative procedure. Based on refining tests, mesh- and time-independent solutions are obtained when 100 equal-spaced volumes and a constant time step equal to 10^{-3} s is used for the space and time discretization, respectively. The numerical procedure used in the solution of the mathematical model consisted of the following steps:

(1) Supply the initial values of the variables ρ_v, p, u, T_f, $\overline{q}_D$, $\overline{q}_d$, T_{SD}, and T_{Sd}.
(2) Solve Eqs. (11) and (12) for each control volume of the column and obtain the adsorbed water concentration ($\overline{q}_D$) and temperature (T_{SD}) for the large particles.
(3) Solve Eqs. (15) and (16) for each control volume of the column and obtain the adsorbed water concentration ($\overline{q}_d$) and temperature (T_{Sd}) for the small particles.
(4) Calculate the pressure field (p) through the mass balance to the moist air (PRIME method).
(5) Calculate the velocity field (u) through the momentum equation.
(6) Calculate the temperature field (T_f) through the energy equation.
(7) Calculate the water vapor density (ρ_v) through the mass balance to the water vapor.
(8) Calculate the moist air density (ρ_f) through the ideal gas law.
(9) Return to Step 2 and iterate until convergence is reached at the current time level.
(10) After convergence, progress to the next time level.
(11) The following criterion is used to verify the convergence of the solution in each time level of the unsteady solution:

$$\left|\frac{\varphi_P^{k+1} - \varphi_P^k}{\varphi_{\max} - \varphi_{\min}}\right| \le 10^{-5} \tag{19}$$

where $\left|\varphi_{\max} - \varphi_{\min}\right|$ denotes the maximum variation of the moist air density field at the kth iteration. If Eq. (19) is not satisfied for each control volume, a new iteration is required.

Before illustrating the results obtained in the present work, the validation of the developed numerical code will be discussed. Due to the lack of experimental data available in the literature to study the dynamics of water vapor adsorption in a silica gel bidisperse bed, the numerical validation

of the model is performed assuming $\delta = 1$ and $x_D = 0$ in the interparticle porosity equation defined in Santos et al. [25]. In this case, the bidisperse model reproduces the particular case of a monodisperse bed for which the experimental results are available in the literature.

Park and Knaebel [28] performed a numerical and experimental study of water vapor adsorption in a silica gel monodisperse bed. Experiments are conducted to obtain equilibrium isotherms and breakthrough curves. Both experiments are performed considering moist air as sorbate at a pressure of 1 atm at temperatures of 25 and 50 °C. The relative humidity at the adsorption column inlet ranged from 6 to 80% during the experimental tests. The authors observed that the inlet relative humidity has a significant influence on the shape of the breakthrough curve. Simple breakthrough curves (sigmoidal shape) were obtained when low humidity (5.8%) was applied, while complex breakthrough forms (dual-shock wave) were produced when high humidity was applied (73%).

In order to test the numerical model developed here, a comparison of our numerical results with the G1C test of Park and Knaebel [28] is performed. This particular case is selected to test the computational code for the reproduction of the most complex forms of the breakthrough curve when high humidity of air is applied to the column inlet. In this case study, a glass column with an outer diameter of 0.0254 m and a length of 0.3 m was considered. Moist air with relative humidity, ϕ_{in}, equal to 73% and temperature, T_{in}, of 25 °C is admitted to the column. Figure 2 shows the comparison of the numerical solution obtained in the present work with the experimental temperature and breakthrough data at the column outlet. The best fit between experimental data and numerical model is obtained when the overall mass transfer coefficient is equal to 1.25×10^{-3} s^{-1} and the overall heat transfer coefficient in the column wall is equal to 4.88 W/ m^2 K. A good agreement between the numerical solution and the experimental data is observed. It is also observed that the model predicted, with reasonable precision, the complex shapes of the breakthrough and temperature curves obtained when high humidity of air is admitted to the adsorption column.

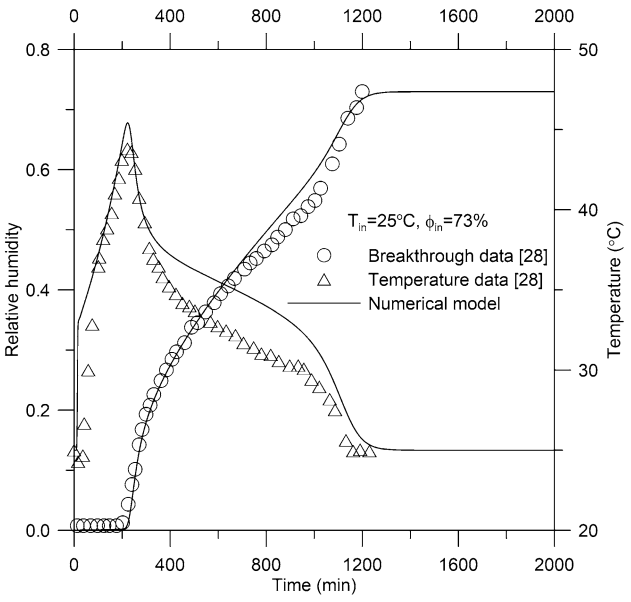

Fig. 2 Comparison between the numerical model of the present work and the experimental data of Park and Knaebel [28] with $\phi_{in} = 73\%$ and $T_{in} = 25$ °C

4 Results and discussion

After the validation of the developed computational code, we now present the numerical results of this work for the adsorption of water vapor in silica gel bidisperse bed. The data and parameters used in the numerical tests are illustrated in Table 1. The performance of the bidisperse bed in the air dehumidification is evaluated through the dehumidification efficiency and the average mass of adsorbed water in the bed. The dehumidification efficiency is given by

$$\eta = \frac{W_{in} - W_{out}}{W_{in}} \tag{20}$$

where W_{in} and W_{out} denote, respectively, the humidity ratios at the inlet and outlet of the column.

4.1 Influence of the particle size ratio on the pressure drop across the bed

For bidisperse beds, as described in Santos et al. [25], the particle size ratio, $\delta = d/D$, influences the interparticle porosity and packing density. If the particle size ratio is reduced, the interparticle porosity decreases and the packing density increases. In addition, reducing the particle size ratio also increases the pressure drop across the bed. In this first case study, the influence of the particle size ratio, δ, on the pressure drop across the bed is investigated. The temperature, T_{in}, and air humidity ratio, W_{in}, at the inlet of the column were equal to 30 °C and 0.025 kg/kg, respectively. The particle size ratio in the bed, δ, assumed the following values: 1 (monodisperse bed), 1/2, 1/5, 1/10, and 1/13. To vary δ, the largest particle size was set at 5 mm and the smallest particle diameter was assumed to be variable and progressively reduced. Three different column sizes were investigated: 0.1, 0.2, and 0.3 m using two different flow rates of the process air: 4.55×10^{-5} kg/s and 1.14×10^{-5} kg/s. Figure 3 shows the effect of the particle size ratio on the pressure drop across the bed. As shown in Fig. 3, the reduction in the particle size ratio of the bidisperse bed

Table 1 Data and physical properties used in the simulations [37, 42]

Larger pellet diameter, D	5 mm
Particle size ratio, $\delta = d/D$	1/13, 1/10, 1/5, 1/2, 1
Intraparticle porosity to the large pellet, ε_{pD}	0.43
Intraparticle porosity to the small pellet, ε_{pd}	0.43
Column length, L	0.1, 0.2, 0.3 m
Column inner radius, R_i	0.0114 m
Initial pressure, p_0	100 kPa
Initial temperature, T_0	30 °C
Pressure drop, $dp = p_{in}$-p_{out}	50, 75, 100 Pa
Inlet temperature, T_{in}	20, 30, 40 °C
Inlet humidity ratio, W_{in}	0.014, 0.015, 0.020, 0.025 kg/ kg
Ideal gas constant to the moist air, R_g	287 J/kg K
Ideal gas constant to the water vapor, R_v	461,4 J/kg K
Adsorbent density, ρ_s	2027 kg/m^3, Ref. [42]
Adsorbent specific heat, C_{ps}	921 J/kg K, Ref. [42]
Effective thermal conductivity of the bed, λ_{ef}	0.198 W/m K, Ref. [42]
Moist air specific heat, C_{pg}	1005 J/kg K
Surrounding temperature, T_∞	30 °C
Adsorption heat, ΔH	-2.693 × 10^6 J/kg, Ref. [37]
Constant of Eq. (19), C_0	7.3 × 10^{-13} kg/kg Pa, Ref. [37]
Constant of Eq. (19), q_∞	0.45 kg/kg, Ref. [37]
Constant of Eq. (19), n	12, Ref. [37]
Constant of Eqs. (11) and (15), D_{S0}	2.54 × 10^{-4} m^2/s, Ref. [42]
Activation energy, E_a	4.2 × 10^4 J/mol, Ref. [42]
Universal gas constant,$\overline{R}$	8.314 J/mol K

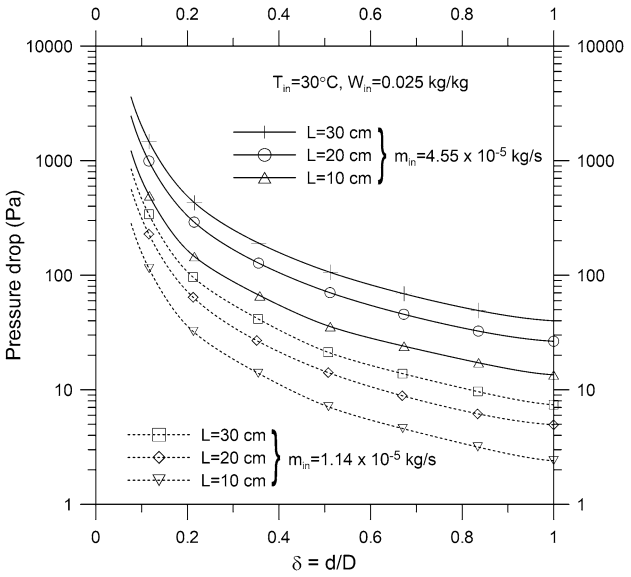

Fig. 3 Effect of the size ratio, δ, on the pressure drop across the bed with $T_{in} = 30$ °C and $W_{in} = 0.025$ kg/kg

increases the pressure drop. In addition, the pressure drop can be decreased by reducing the size of the column or reducing the applied air flow rate.

4.2 Influence of size ratio on dehumidification efficiency and adsorption capacity

In this case study, the influence of the particle size ratio, δ, on the air dehumidification process is investigated. The temperature, T_{in}, and air humidity ratio, W_{in}, at the inlet of the column were equal to 30 °C and 0.025 kg/kg, respectively. The particle size ratio in the bed, δ, assumed the following values: 1 (monodisperse bed), 1/2, 1/5, 1/10, and 1/13. Reducing the size ratio, δ, reduces bed porosity along with the flow rate applied to the column. Thus, to keep the air flow constant ($m_{in} = 4.55 \times 10^{-5}$ kg/s) at the column inlet, five distinct inlet pressure values were considered: 100.04, 100.11, 100.49, 102.01, and 103.6 kPa. These values correspond, respectively, to the following size ratios: $\delta = 1$; 1/2;

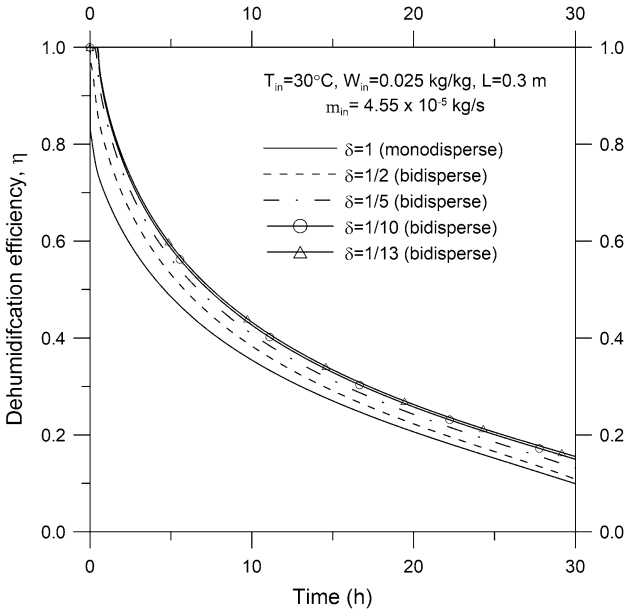

Fig. 4 Influence of size ratio, δ, on dehumidification efficiency with $T_{in}=30$ °C, $W_{in}=0.025$ kg/kg, $m_{in}=4.55\times10^{-5}$ kg/s, and $L=0.3$ m

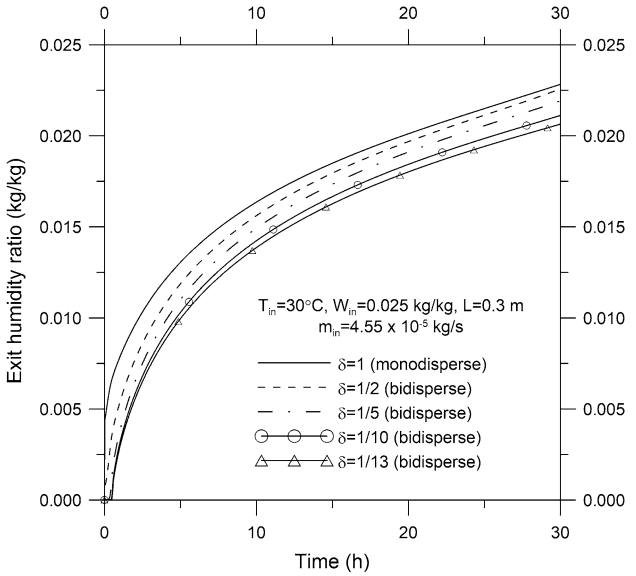

Fig. 5 Influence of size ratio, δ, on the air outlet humidity ratio with $T_{in}=30$ °C, $W_{in}=0.025$ kg/kg, $m_{in}=4.55\times10^{-5}$ kg/s, and $L=0.3$ m

1/5, 1/10, and 1/13. The pressure at the column outlet was kept constant and equal to 100 kPa.

Figure 4 shows the influence of pellet size ratio on the dehumidification efficiency of the silica gel bidisperse bed. It is observed that the dehumidification efficiency of the monodisperse bed ($\delta=1$) is smaller when compared to the bidisperse bed configuration. For example, after 5 h, the efficiency of the monodisperse bed drops to about 0.48, while the efficiency of the bidisperse bed reaches about 0.59 (improvement in performance of 22.9%) for $\delta=1/13$, which corresponds to the maximum packing density investigated. Bidisperse packing increases the packing density and the amount of silica in the bed. Therefore, the dehumidification efficiency of the bidisperse bed is higher because the moisture retention in the column is increased by the additional amount of desiccant material added to the bed. However, as we can see from Fig. 4 there is not much difference from the dehumidification results obtained with δ equal to 1/10 and 1/13. We can justify such behavior by considering that when the compaction of silica gel is increased, the porosity and absolute permeability of the column decreases; consequently, the mass transfer in the column decreases. Therefore, there is minimum value that δ can be reduced and then $\delta=1/10$ is adopted as optimal size ratio for application in the bidisperse bed.

Figures 5 and 6 show the influence of the size ratio, δ, on the humidity ratio and air temperature at the column outlet. As shown in Fig. 5, the reduction in δ results in a progressive reduction in the humidity of the air leaving the column that contributes to the increment of the dehumidification capacity of the bed. Figure 6 shows that the air temperature at the outlet of the column increases when δ decreases, indicating an increase in the amount of sensible heat present in the air. Such behavior occurs because when δ decreases, the amount of adsorbent increases, and therefore also increases the amount of heat released in the adsorption process. Although the outlet temperature obtained with the bidisperse bed was close to 58 °C, when $\delta=1/10$ was used, studies have shown

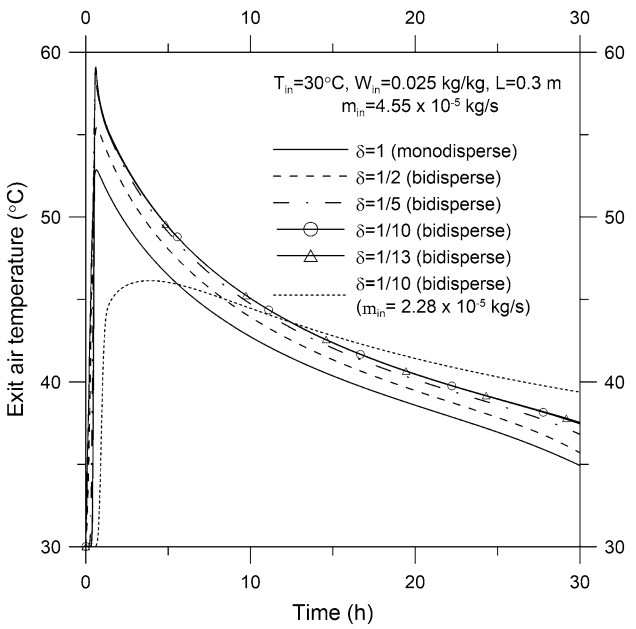

Fig. 6 Influence of size ratio δ on the exit air temperature with $T_{in}=30$ °C, $W_{in}=0.025$ kg/kg, $m_{in}=4.55\times10^{-5}$ kg/s, and $L=0.3$ m

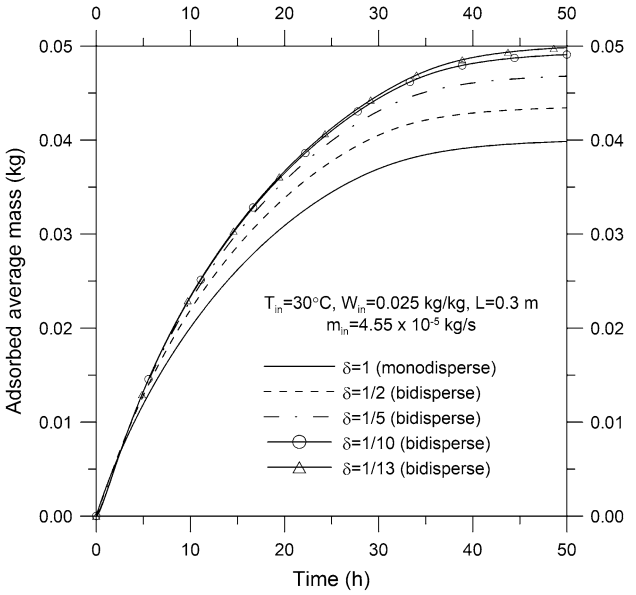

Fig. 7 Influence of size ratio, δ, on the average mass of adsorbed water with $T_{in}=30$ °C, $W_{in}=0.025$ kg/kg, $m_{in}=4.55\times10^{-5}$ kg/s, and $L=0.3$ m

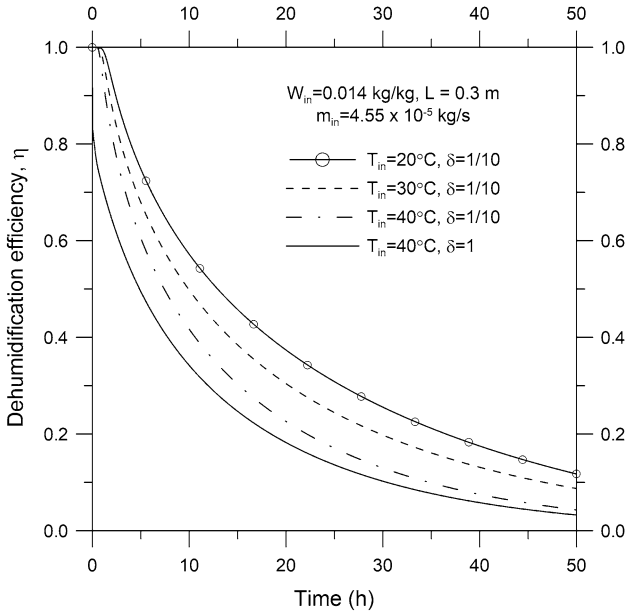

Fig. 8 Influence of process air temperature on bidisperse bed dehumidification efficiency with $\delta=1/10$, $W_{in}=0.014$ kg/kg, $m_{in}=4.55\times10^{-5}$ kg/s, and $L=0.3$ m

that it is still possible to obtain thermal comfort, in this case, through the use of efficient regenerative heat exchangers and evaporative coolers [48–50]. In addition, if the applied air flow rate is reduced, the outlet air temperature is also decreased. As it can be verified in Fig. 6, when the applied air flow rate was reduced by half, the outlet temperature was decreased from 58 °C to 47 °C, for $\delta=1/10$.

Figure 7 shows the effect of the size ratio, δ, on the average mass of adsorbed water in the bed. Comparing the results of monodisperse with the bidisperse bed configuration, it is observed that the adsorption kinetics in the monodisperse column ($\delta=1$) is faster, and hence, the bed saturates in a shorter time interval. This is due to the low packing density of the monodisperse bed and the lower amount of compacted silica. Since saturation of the monodisperse bed is faster, its dehumidification efficiency is smaller. When $\delta=1/13$ and the bed saturation is reached, it is also observed that the bidisperse bed adsorption capacity is 25% greater than that obtained with the monodisperse bed.

4.3 Influence of process air temperature

In the previous section, it was observed that the bidisperse bed is more efficient than the monodisperse bed for the air dehumidification process. For all cases investigated next, $\delta=1/10$ will be considered for the bidisperse bed, since this size ratio represents a good compromise between dehumidification efficiency and pressure drop applied to the column. In this section, the influence of process air temperature on dehumidification capacity will be investigated. The air humidity ratio at the inlet of the column was considered equal to 0.014 kg/kg while the process air temperature at the inlet was assumed to be the following values: 20, 30, and 40 °C. The air pressure at the inlet of the column is equal to 102.01 kPa while the outlet pressure is equal to 100 kPa.

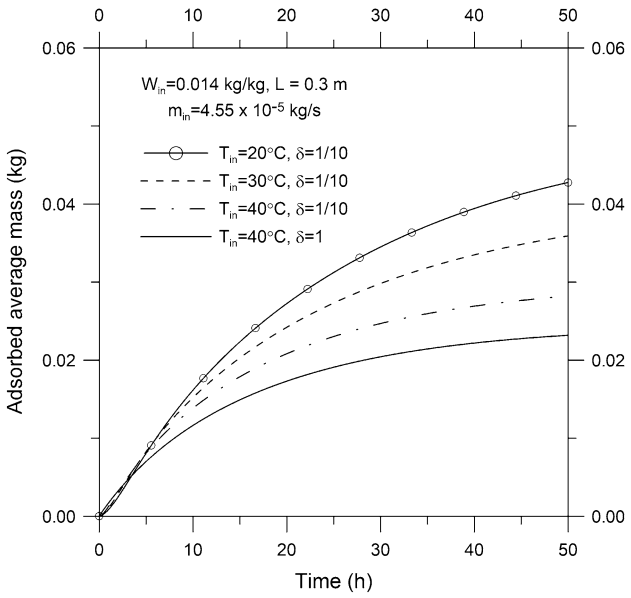

Fig. 9 Effect of process air temperature on bidisperse bed adsorption capacity with $\delta=1/10$, $W_{in}=0.014$ kg/kg, $m_{in}=4.55\times10^{-5}$ kg/s, and $L=0.3$ m

In this condition, the pressure drop applied imposes an air flow rate at the inlet of the column equal to 4.55×10^{-5} kg/s.

Figure 8 shows the effect of process air temperature on the dehumidification efficiency of the bidisperse bed. As expected, it is observed that raising the process air temperature reduces the dehumidifying efficiency of the bed. This is because raising the process air temperature reduces the adsorption capacity of the bed, as shown in Fig. 9, which also reduces the performance in terms of dehumidification. It is also shown in Figs. 8 and 9 a comparison between the performance obtained for monodisperse ($\delta = 1$) and bidisperse ($\delta = 1/10$) beds under hot weather conditions ($T_{in} = 40$ °C). From Fig. 8, it is observed that the efficiency of the monodisperse bed is always lower than that of the bidisperse bed. This occurs because the monodisperse bed saturates faster and adsorbs a smaller amount of water than the bidisperse bed, as it can be observed in Fig. 9.

4.4 Influence of process air humidity ratio

In this case study, the influence of the process air humidity ratio on the dehumidification efficiency and adsorption capacity of the bidisperse bed is investigated. The process air temperature at the column inlet is equal to 30 °C. Three distinct values of humidity ratio are assumed for the process air at the column inlet: 0.015, 0.020, and 0.025 kg/kg. The inlet air pressure of the column is equal to be 102.01 kPa, while the outlet pressure is equal to 100 kPa. In this situation, the mass flow rate applied is equal to 4.55×10^{-5} kg/s. Figure 10 shows the effect of process air humidity ratio on the dehumidification efficiency of the bidisperse bed. In this figure, it is observed that increasing the humidity of the process air reduces the dehumidification efficiency of the bed. However, even in the case of high process air humidity ($W_{in} = 0.025$ kg/kg), after 25 h of operation, it is observed that the dehumidification efficiency is very similar to that recorded for cases where lower humidity is considered, reaching around 20%. This indicates that the bidisperse bed maintains its dehumidifying capacity even when a high humidity condition of the process air is considered. This is an important and necessary feature for lowering the latent load in the desiccant air conditioning systems, especially in hot and humid climates where the latent load is high. However, the above statement does not apply to the monodisperse bed. Figure 10 also shows that the efficiency of the monodisperse bed is smaller when high humidity is applied to the column. This behavior can be explained with the help of Fig. 11, where the influence of process air humidity on bed adsorption capacity is presented. It is observed that the adsorption capacity of the monodisperse bed is very limited because the bed saturates quickly when high humidity is applied.

4.5 Influence of pressure drop

In this section, the influence of the pressure drop (flow rate) applied to the column is investigated. The outlet pressure is kept at 100 kPa, while the following pressures drops are applied to the adsorbent column: 50 ($m_{in} = 3.77 \times 10^{-6}$ kg/s), 75 ($m_{in} = 5.63 \times 10^{-6}$ kg/s) and 100 Pa ($m_{in} = 2.32 \times 10^{-5}$

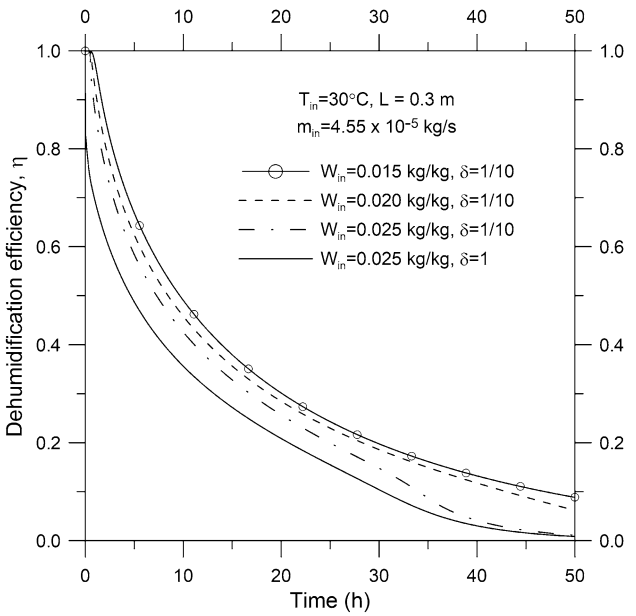

Fig. 10 Influence of process air humidity on bidisperse bed dehumidification efficiency with $\delta = 1/10$, $T_{in} = 30$ °C, $m_{in} = 4.55 \times 10^{-5}$ kg/s, and $L = 0.3$ m

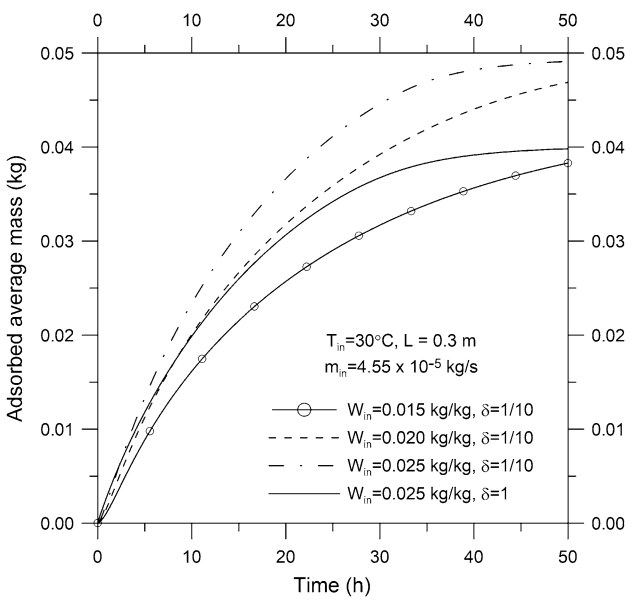

Fig. 11 Influence of process air humidity on bidisperse bed adsorption capacity with $\delta = 1/10$, $T_{in} = 30$ °C, $m_{in} = 4.55 \times 10^{-5}$ kg/s, and $L = 0.3$ m

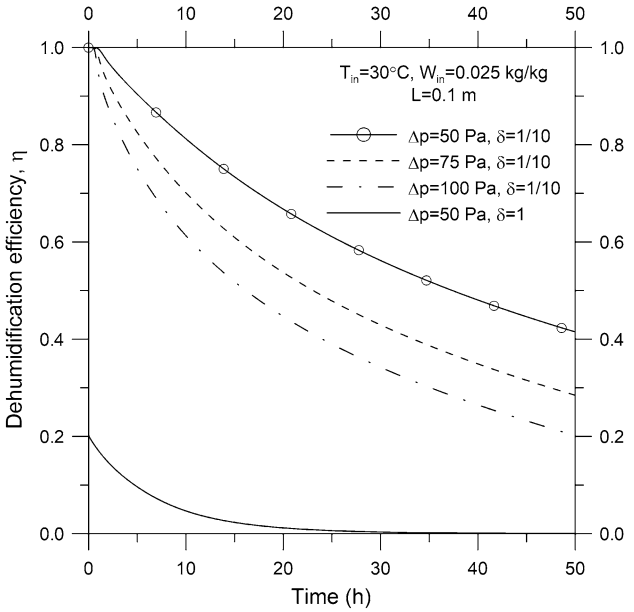

Fig. 12 Influence of pressure drop on bidisperse bed dehumidification efficiency with δ = 1/10, W_{in} = 0.025 kg/kg, T_{in} = 30 °C, and L = 0.1 m

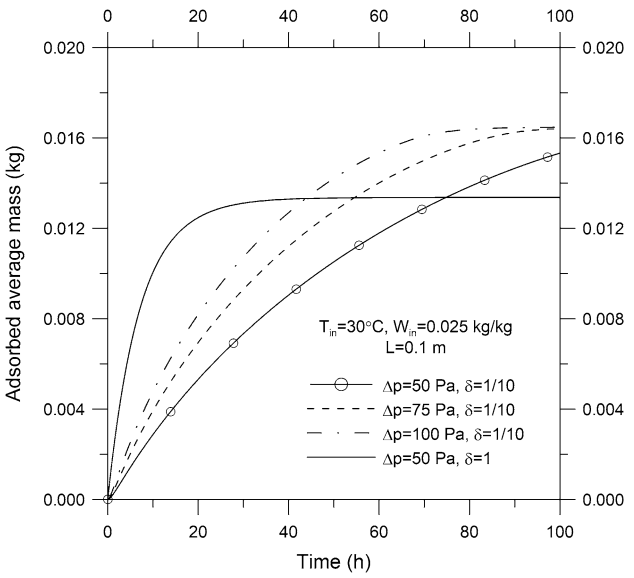

Fig. 13 Influence of pressure drop on bidisperse bed adsorption capacity with δ = 1/10, W_{in} = 0.025 kg/kg, T_{in} = 30 °C, and L = 0.1 m

kg/s). The temperature and humidity ratio of the process air at the inlet column are equal to 30 °C and 0.025 kg/kg, respectively. The column length was equal to 0.1 m. It can be seen in Fig. 12 that the dehumidification efficiency of the bidisperse bed is reduced when the pressure drop applied to the bed increases. This occurs because when the pressure drop increases, the amount of water vapor present in the process air increases, since the air flow admitted to the column is also increased. Henceforth, as shown in Fig. 13, when the pressure drop increases, the adsorption kinetics in the column occur faster and the bed saturates more rapidly. Under these conditions, the bed loses its water vapor adsorption capacity and the dehumidification efficiency decreases rapidly. Figures 12 and 13 also shows a performance comparison between monodisperse and bidisperse bed when the pressure drop applied to the column is equal to 50 Pa. For this pressure drop, as observed in Fig. 12, the reduction in dehumidification performance of the monodisperse bed is much more severe than the one in the bidisperse bed. This is because the monodisperse bed saturates much faster than the bidisperse bed for the same pressure drop applied, as observed in Fig. 13.

5 Conclusions

In the present work, a numerical study of the water vapor adsorption dynamics in silica gel bidisperse bed was performed. Bidisperse packing was proposed as a way to increase the dehumidifying capacity of air in desiccant beds by increasing the amount of adsorbed water vapor. A numerical model for the description of the water vapor adsorption dynamics in a silica gel bidisperse bed was developed and the finite volume method was used to solve the mass, momentum, and energy balances in the adsorbent column. The influence of the particle size ratio on the pressure drop across the bed was first investigated. The numerical results showed that the reduction in the particle size ratio, δ, of the bidisperse bed increases the pressure drop. In addition, a reduction in the pressure drop can be obtained by reducing the size of the column or by reducing the applied air flow rate. The numerical results also showed that the reduction of the size ratio, δ, in the adsorbent particles increases the air dehumidification efficiency due to the improvement of the water vapor adsorption capacity. Comparing the results of the bidisperse bed, when $\delta = 1/13$ was assumed, with the monodisperse case, a gain of about 23% was obtained in the bidisperse bed dehumidification efficiency while adsorption capacity was 25% greater. However, there is minimum value that δ can be reduced without decrease the mass transfer in the bed; δ = 1/10 was identified as the optimal size ratio for application in the bidisperse bed. The influence of temperature and humidity conditions of process air on bidisperse bed dehumidification efficiency was also investigated. Increasing the temperature and humidity of the process air has been observed to reduce the bed dehumidification efficiency. However, the decrease in efficiency was small when high humidity was applied, and it can be concluded that the bidisperse bed maintains its potential for air dehumidification under humid climate conditions, where the latent load

of process air is high. The effect of pressure drop applied to the bidisperse bed was also studied. When the pressure drop applied is high, the air flow rate increases, and the efficiency of the bidisperse bed decreases. However, for the same pressure drop applied, the drop in performance of the monodisperse bed is much more severe than the one in the bidisperse bed due to its low packing density and adsorption capacity. In general, it can be concluded that the use of bidisperse packing in the desiccant bed can contribute to the improvement of the coefficient of performance (COP) in desiccant air conditioning systems as the efficiency of the dehumidification process and the adsorption capacity increases relative to the case where monodisperse packing is considered.

Acknowledgements The authors thank the CNPq (The National Council for Scientific and Technological Development of Brazil) and FUNCAP (The Foundation to Support the Scientific and Technological Development of Ceará-Brazil) for their financial support through grants (308865/2016-2 and 305851/2015-2) and (BP3-0139-00332.01.00/18), respectively.

References

1. Al-Alili A, Hwang Y, Radermacher R (2014) Review of solar thermal air conditioning technologies. Int J Refrig 39:4–22
2. Enteria N, Mizutani K (2011) The role of the thermally activated desiccant cooling technologies in the issue of energy and environment. Renew Sustain Energy Rev 15:2095–2122
3. Zheng X, Ge TS, Wang RZ (2014) Recent progress on desiccant materials for solid desiccant cooling systems. Energy 74:280–294
4. Jeong JW, Mumma AS (2005) Practical thermal performance correlations for molecular sieve and silica gel loaded enthalpy wheels. Appl Therm Eng 25:719–740
5. Jia CX, Dai YJ, Wang RZ (2007) Use of compound desiccant to develop high performance desiccant cooling system. Int J Refrig 30:345–353
6. Choudhury B, Saha BB, Chatterjee PK, Sarkar JP (2013) An overview of developments in adsorption refrigeration systems towards a sustainable way of cooling. Appl Energy 104:554–567
7. Mazzei P, Minichiello F, Palma D (2005) HVAC dehumidification systems for thermal comfort: a critical review. Appl Therm Eng 25:677–707
8. Zhang LZ, Niu JL (2002) Performance comparisons of desiccant wheels for air dehumidification and enthalpy recovery. Appl Therm Eng 22:1347–1367
9. Yeboah SK, Darkwa J (2016) A critical review of thermal enhancement of packed beds for water vapor adsorption. Renew Sustain Energy Rev 58:1500–1520
10. Freni A, Tokarev MM, Restuccia G, Okunev AG, Aristov YI (2002) Thermal conductivity of selective water sorbents under the working conditions of a sorption chiller. Appl Therm Eng 22:1631–1642
11. Sharafian A, McCague C, Bahrami M (2015) Impact of fin spacing on temperature distribution in adsorption cooling system for vehicle A/C applications. Int J Refrig 51:135–143
12. Girnik IS, Aristov YI (2016) Making adsorptive chillers more fast and efficient: the effect of bi-dispersed adsorbent bed. Appl Therm Eng 106:254–256
13. Ben Aim R, LeGoff P, Le Lec P (1971) La perméabilité de milieux poreux formés par empilement de mélanges binaires de grains sphériques. Powder Technol 5:51–60
14. Standish N, Mellor DG (1980) The permeability of ternary coke mixtures. Powder Technol 27:61–68
15. Standish N, Collins DN (1983) The permeability of ternary particulate mixtures for laminar flow. Powder Technol 36:55–60
16. Leitzelement M, Lo CS, Dodds J (1985) Porosity and permeability of ternary mixtures of particles. Powder Technol 41:159–164
17. MacDonald MJ, Chu CF, Guilloit PP, Ng KM (1991) A generalized Blake-Kozeny equation for multisized spherical particles. AIChE J 37:1583–1588
18. Mota M, Teixeira JA, Yelshin A (2001) Binary spherical particle mixed beds porosity and permeability relationship measurement. Trans Filtration Soc 1:101–106
19. Dias RP, Fernandes CS, Mota M, Teixeira JA, Yelshin A (2007) Permeability and effective thermal conductivity of bisized porous media. Int J Heat Mass Transf 50:1295–1301
20. Dias RP, Fernandes CS, Teixeira JA, Mota MG, Yelshin AI (2008) Permeability analysis in bisized porous media: wall effect between particles of different size. J Hydrol 349:470–474
21. Tsotsas E, Martin H (1987) Thermal conductivity of packed beds: a review. Chem Eng Process 22:19–37
22. Tsotsas E, Schluender EU (1990) Numerical calculation of the thermal conductivity of two regular bi-dispersed beds of spherical particles. Comput Chem Eng 14:1031–1038
23. Chang CH (1994) Packing adsorbent particles for storage of natural gas. U.S. Patent 5,308,821
24. Shirley AI, LaCava AI (1995) PSA performance of densely packed adsorbent beds. AIChE J 41:1389–1394
25. Santos JC, Lima JA, Gurgel JM, Marcondes F (2019) Improvement of methane storage capacity in activated carbon bed with bidisperse packing. Braz J Chem Eng 36:831–843
26. Pesaran AA, Mills AF (1987) Moisture transport in silica gel packed beds-I. Theoretical study. Int J Heat Mass Transf 30:1037–1049
27. Pesaran AA, Mills AF (1987) Moisture transport in silica gel packed beds-II. Experimental study. Int J Heat Mass Transf 30:1051–1060
28. Park I, Knaebel KS (1992) Adsorption breakthrough behavior: unusual effects and possible causes. AIChE J 38:660–670
29. Sun J, Besant RW (2005) Heat and mass transfer during silica gel-moisture interactions. Int J Heat Mass Transf 48:4953–4962
30. Nastaj J, Ambrozek B (2009) Modeling of drying of gases using solid desiccants. Drying Technol 27:1344–1352
31. Ramzy AK, Kadoli R, Babu A (2011) Improved utilization of desiccant material in packed bed dehumidifier using composite particles. Renewable Energy 36:732–742
32. Ramzy AK, Kadoli R, Babu A (2011) Semi-analytical method for heat and moisture transfer in packed bed of silica gel. Int J Heat Mass Transf 54:983–993
33. Ramzy AK, Kadoli R, Babu A (2013) Experimental and theoretical investigations on the cyclic operation of TSA cycle for air dehumidification using packed beds of silica gel particles. Energy 56:8–24
34. Zouaoui A, Zili-Guedira L, Nasrallah SB (2017) Solid desiccant solar air conditioning unit in Tunisia: numerical study. Int J Refrig 74:662–681
35. Erdogan M, Bau U, Bardow A (2019) Benchmarking commercial adsorbents for drying air in a packed bed. Appl Therm Eng 1(160):113942
36. Wakao N, Funazkri T (1978) Effect of fluid dispersion coefficients on particle-to-fluid mass transfer coefficients in packed beds. Chem Eng Sci 33:1375–1384
37. Sakoda A, Suzuki M (1984) Fundamental study on solar powered adsorption cooling system. J Chem Eng Jpn 17:52–57

38. Sun LM, Meunier F (1987) A detailed model for nonisothermal sorption in porous adsorbents. Chem Eng Sci 42:1585–1593
39. Gurgel JM, Andrade Filho LS, Grenier PH, Meunier F (2001) Thermal diffusivity and adsorption kinetics of silica gel/water. Adsorption 7:211–219
40. Santos JC, Gurgel JM, Marcondes F (2015) Numerical simulation of fast charge of natural gas on activated carbon in conjunction with variable velocity. Appl Therm Eng 90:258–265
41. Tóth J (1971) State equations of the solid-gas interface layers. Acta Chem Acad Sci Hung 69:311
42. Chua HT, Ng KC, Wang W, Yap C, Wang XL (2004) Transient modeling of a two-bed silica gel-water adsorption chiller. Int J Heat Mass Transf 47:659–669
43. Maliska CR (2004) Heat transfer and computational fluid mechanics, 2n edn. Editora LTC, Florianópolis (in Portuguese)
44. Patankar SV (1980) Numerical heat transfer and fluid flow. Hemisphere, New York
45. Maliska CR (1981) A solution method three-dimensional parabolic fluid flow problems in nonorthogonal coordinates, Ph. D. Thesis, University of Warterloo, Warterloo, Canada
46. Raithby GD, Torrance KE (1974) Upstream-weight differencing schemes and their application to elliptic problems involving fluid flows. Comput Fluids 2:191–206
47. Marcondes F, Maliska CR (1999) Treatment of the inlet boundary conditions in natural convection flows in open-ended channels. Num Heat Transfer Part B 35:317–345
48. Khalid A, Mahmood M, Asif M, Muneer T (2009) Solid assisted, pre-cooled hybrid desiccant cooling system for Pakistan. Renewable Energy 34:151–157
49. Enteria N, Yoshino H, Satake A, Mochida A, Takaki R, Yoshie R, Baba S (2010) Development and construction of the novel solar thermal desiccant cooling system incorporating hot water production. Appl Energy 87:478–486
50. El-Agouz SA, Kabeel AE (2014) Performance of desiccant air conditioning system with geothermal energy under different climatic conditions. Energy Convers Manage 88:464–475